Cell

Biomechanical Remodeling of the Microenvironment by Stromal Caveolin-1 Favors Tumor Invasion and Metastasis

Jacky G. Goetz,[1,7,8,*] Susana Minguet,[1,7] Inmaculada Navarro-Lérida,[1] Juan José Lazcano,[1] Rafael Samaniego,[3] Enrique Calvo,[2] Marta Tello,[4] Teresa Osteso-Ibáñez,[1] Teijo Pellinen,[1] Asier Echarri,[1] Ana Cerezo,[1] Andres J.P. Klein-Szanto,[6] Ricardo Garcia,[4] Patricia J. Keely,[5] Paloma Sánchez-Mateos,[3] Edna Cukierman,[6] and Miguel A. Del Pozo[1,*]

[1]Integrin Signaling Laboratory, Department of Vascular Biology and Inflammation
[2]Proteomics Unit
Centro Nacional de Investigaciones Cardiovasculares (CNIC), Madrid 28029, Spain
[3]Laboratorio de Inmuno-oncología/Unidad de Microscopía Confocal, Hospital General Universitario Gregorio Marañón, Madrid 28007, Spain
[4]Forcetool Group, Instituto de Microelectrónica de Madrid, Consejo Superior de Investigaciones Científicas (CSIC), Tres Cantos 28760, Spain
[5]Laboratory of Molecular Biology, Department of Pharmacology, University of Wisconsin, Madison, WI 53706, USA
[6]Cancer Biology Program, Philadelphia, PA 19111, USA
[7]These authors contributed equally to this work
[8]Present address: Institute of Genetics and Molecular and Cellular Biology, Illkirch 67404, France
*Correspondence: jgoetz@igbmc.fr (J.G.G.), madelpozo@cnic.es (M.A.D.P.)
DOI 10.1016/j.cell.2011.05.040

SUMMARY

Mechanotransduction is a key determinant of tissue homeostasis and tumor progression. It is driven by intercellular adhesions, cell contractility, and forces generated within the microenvironment and is dependent on extracellular matrix composition, organization, and compliance. We show that caveolin-1 (Cav1) favors cell elongation in three-dimensional cultures and promotes Rho- and force-dependent contraction, matrix alignment, and microenvironment stiffening through regulation of p190RhoGAP. In turn, microenvironment remodeling by Cav1 fibroblasts forces cell elongation. Cav1-deficient mice have disorganized stromal tissue architecture. Stroma associated with human carcinomas and melanoma metastases is enriched in Cav1-expressing carcinoma-associated fibroblasts (CAFs). Cav1 expression in breast CAFs correlates with low survival, and Cav1 depletion in CAFs decreases CAF contractility. Consistently, fibroblast expression of Cav1, through p190RhoGAP regulation, favors directional migration and invasiveness of carcinoma cells in vitro. In vivo, stromal Cav1 remodels peri- and intratumoral microenvironments to facilitate tumor invasion, correlating with increased metastatic potency. Thus, Cav1 modulates tissue responses through force-dependent architectural regulation of the microenvironment.

INTRODUCTION

In vivo, cells interact with a three-dimensional (3D) microenvironment (Yamada and Cukierman, 2007). The mechanical force of these interactions, by altering tissue tension, acts as a molecular switch that determines cell fate (Engler et al., 2009). Tension generated in an extracellular microenvironment induces and cooperates with opposing forces applied by cells (mechanoreciprocity). In embryogenesis such tensile forces govern tissue organization (Krieg et al., 2008), and mammary acinar architecture relies on matrix compliance and cell tension (Ronnov-Jessen and Bissell, 2008).

Microenvironment-mediated tensile forces also contribute to disease. Matrix stiffness promotes breast cancer progression via mechanoreciprocal induction of Rho-dependent cell contractility (Levental et al., 2009). The microenvironment is also important for tumor invasion and metastasis: tumor cells (TCs) migrate along tracks made of extracellular matrix (ECM) collagen fibers (Friedl and Gilmour, 2009), and whereas reticular collagen surrounding mammary glands restrains invasion, Rho-mediated alignment of dense collagen fibers perpendicular to the tumor boundary promotes it (Provenzano et al., 2008). Activated fibroblasts facilitate tumor cell invasion through protease- and force-dependent generation of ECM tracks (Gaggioli et al., 2007). Carcinoma-associated fibroblasts (CAFs) and mesenchymal stem cells, via paracrine cytokine signaling, promote tumor growth, invasion, and metastasis (Karnoub et al., 2007; Orimo et al., 2005). Elucidation of tumor microenvironment remodeling mechanisms is thus an important area of research.

Caveolin-1 (Cav1), the major component of endocytic caveolae plasma membrane (PM) invaginations, has many functions outside caveolae (Parton and Simons, 2007). Cav1 activates

Rho by regulating its endogenous inhibitor p190RhoGAP (p190) and assists in focal adhesion (FA) stabilization required for directional cell migration (Goetz et al., 2008a; Grande-Garcia et al., 2007). The role of Cav1 in tumor progression remains unclear. In most primary tumors Cav1 levels decrease, allowing proliferation, anchorage independence, and angiogenesis, whereas metastasis correlates with Cav1 re-expression, promoting invasion, survival, and multidrug resistance (Goetz et al., 2008b). Most studies have focused on Cav1 expression in TCs, with little attention paid to a possible role in the tumor microenvironment. Because Cav1, via a mechanism involving Cav1 Tyr14 and p190, is essential for fibroblast function (Grande-Garcia et al., 2007), we investigated the role of fibroblast-Cav1 in stroma assembly.

We show that Cav1 regulates Rho GTPase activity by modulating membrane partitioning of p190 and thereby its phosphorylation. Fibroblast expression of Cav1 in vitro and in vivo favors an organized 3D stromal architecture that promotes spindle morphology, facilitates TC invasion, and increases p190-dependent metastatic potency. These findings correlate with increased numbers of Cav1-expressing CAFs in the stroma of human tumor samples. Cav1 silencing in human CAFs decreases their contractility, identifying a role for Cav1 in normal tissue homeostasis and pathological scenarios.

RESULTS

Cav1 Regulates Matrix-Induced Cell Morphology and Reciprocal Interaction with the 3D Microenvironment through Contraction

For a physiologically realistic culture substrate, we generated cell-free 3D matrices from confluent 8 day fibroblasts cultured in the presence of ascorbic acid; the resulting fibroblast-derived 3D matrices (FDMs) are rich in fibronectin (FN) and closely resemble in vivo mesenchymal matrices (Figure 1A, Figure S1A available online, and Movie S1). We seeded FDMs with Cav1 wild-type (Cav1WT) and Cav1 knockout (Cav1KO) mouse embryonic fibroblasts (MEFs) and analyzed cell morphology. Growth in FDMs doubled the cell length:breadth ratio (elliptical factor/EF) of Cav1WT MEFs (Figure 1B and Figure S1B) and almost halved their surface area compared with growth on 2D FN (Figure S1C). In contrast, FDM culture only mildly affected the morphology of Cav1KO MEFs, though it increased the number of cell protrusions (Figures 1B and 1C). Similar results were obtained when cells were grown in collagen-I (Col-I) gels (Figure 1D, Movie S2, and Movie S3).

Consistent with Cav1-dependent Rac regulation (Grande-Garcia et al., 2007), Cav1 deficiency increased PM targeting of Rac1 and its downstream effector phospho-S141-Pak1 (Figure 1E and Figure S1D). In contrast, phosphorylation of myosin light chain-2 (pMLC) was decreased (not shown), suggesting that Cav1 influences cell-induced matrix contractility. Consistently, Cav1WT MEFs contracted Col-I gels more effectively than Cav1KO MEFS at all cell concentrations tested (Figure 1F and Figure S1E). Re-expression of unmodified Cav1, but not its nonphosphorylatable mutant Cav1Y14F, rescued Rac1 localization, cell elongation, gel contraction, and pMLC levels in Cav1KO MEFs (Figure 1G and data not shown). Cav1 thus regulates features of fibroblasts that influence mechanical 3D microenvironment remodeling.

Cav1-Dependent Microenvironment Regulates Cell Shape, Protrusion Number, Rac1 Activity, and Morphology of Integrin-Dependent Adhesion Structures

To test the role of Cav1 in 3D microenvironment formation, we compared culture in FDMs produced from immortalized Cav1WT and Cav1KO MEFs with 2D culture. Three-dimensional growth raised smooth muscle actin (SMA) expression preferentially in WT MEFs close to levels in primary cultures (pMEFs) (Figure S2A). When these FDMs were reseeded with Cav1WT or Cav1KO MEFs, cells of both genotypes were more elongated when grown in FDMs generated by WT MEFs (Figure 2B and Figure S2B). These results suggest that lack of Cav1 alters FDM structure and composition; the most elongated cells were obtained when Cav1WT MEFs were plated in Cav1WT FDMs. Re-expression of Cav1 in Cav1KO MEFs rescued the ability to generate pro-elongation 3D matrices, whereas re-expression of Cav1Y14F had no effect (Figures 2C and 2D). Thus Cav1, through residue Tyr14, favors fibroblast elongation directly through endogenous expression and indirectly through cell-dependent 3D microenvironment remodeling, indicating that endogenous Cav1 and the Cav1-dependent microenvironment cooperate to enhance cell polarity. Cav1WT FDMs also reduced the number of cell protrusions (Figure 2E and Figure S2C) and Rac-GTPase activity (Figure 2F) independently of Cav1 expression by seeded cells, confirming the ability of Cav1-dependent ECM to favor in vivo-like spindle morphology.

We next assessed the impact of the Cav1-dependent microenvironment on the formation of 3D-matrix adhesions. Integrin-dependent 3D-matrix adhesions differ from regular FA in molecular composition (lower pY397FAK levels) and are longer (up to 19 μm) and thinner (Cukierman et al., 2001). Cav1WT and Cav1KO FDMs both decreased adhesion-targeted pY397FAK levels compared to a 2D FN substrate (Figure S2D). The longest 3D-matrix adhesions were obtained when Cav1WT MEFs were plated in Cav1WT FDMs (11.14 ± 0.48 μm) (Figure 2G and Figure S2E), indicating that both matrix and cells are important for determining adhesion length. The matrix adhesion marker vinculin localizes to 3D-matrix adhesions and its recruitment is force dependent (Cukierman et al., 2001), and the mobile vinculin fraction, determined by fluorescence recovery after photobleaching (FRAP), is an index of adhesion-dependent force increase (Bershadsky et al., 2003). Cav1KO FDMs increased the mobile vinculin fraction (Figures 2Ha–2Hc), indicating that these matrices slow the maturation of adhesion structures and the generation of adhesion-dependent forces. Endogenous Cav1 expression contributes little to the maturation of 3D-matrix adhesions (Figures 2Hb and 2Hc), contrasting the strong influence of the assorted FDMs.

Cav1 Promotes Patterning and Stiffness of 3D Matrices thus Regulating Normal Tissue Architecture

To assess the impact of Cav1 expression on microenvironment organization, compliance, and composition, we measured FN fiber orientation in FDMs. FN fibers in Cav1WT-derived FDMs were more parallel than in Cav1KO FDMs (Figures 3A and 3B).

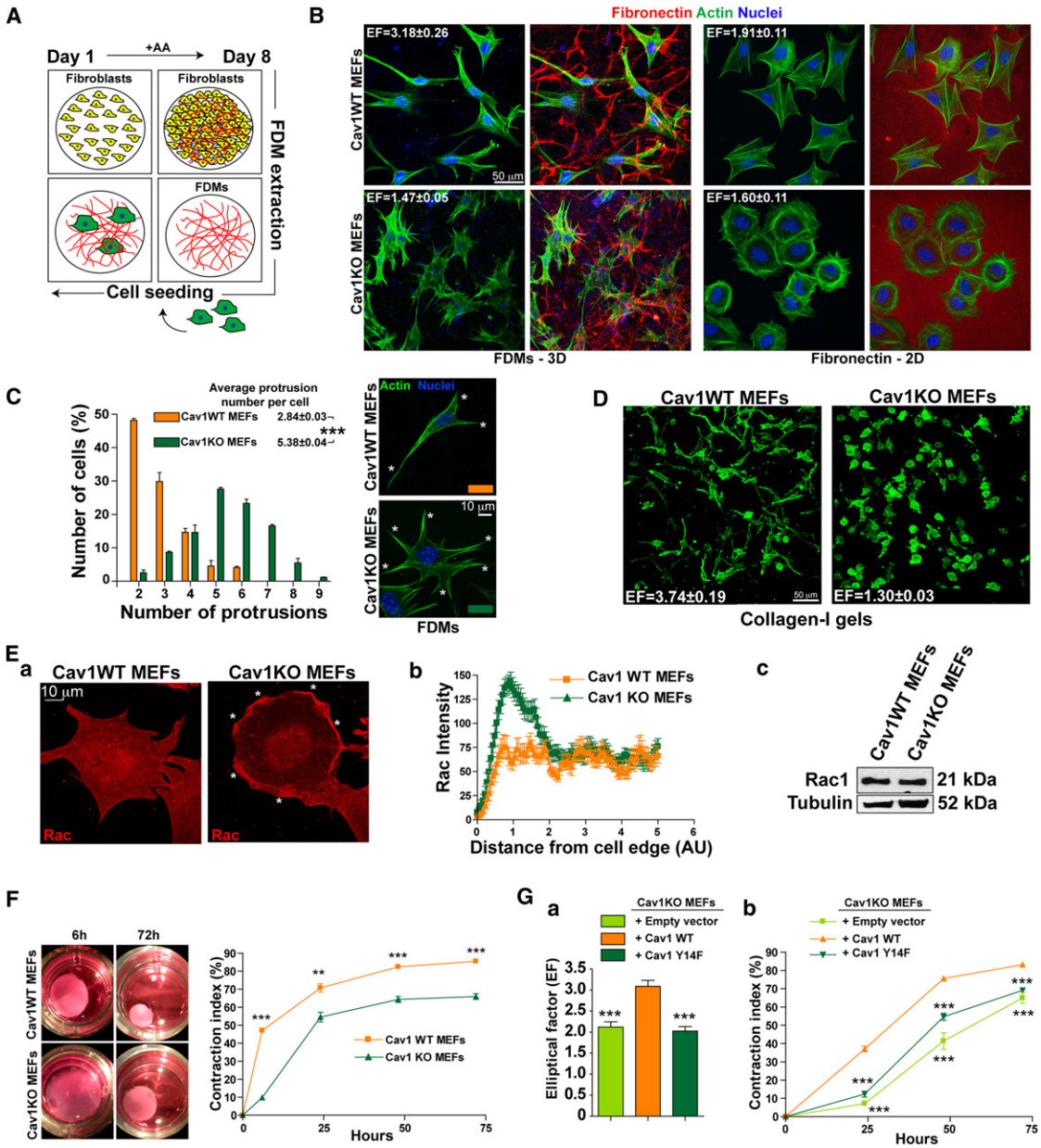

Figure 1. Cav1-Regulated Contractility Controls Matrix-Induced Cell Morphology and Reciprocal Interaction with the 3D Microenvironment

(A) FDMs were generated from NIH 3T3 cells cultured with daily ascorbic acid (AA) supplement.

(B) Cav1WT and KO MEFs were plated (4 hr) on NIH 3T3 FDMs (3D) or FN (5 μg/ml, 2D) and labeled as indicated. Elliptical factors (EF) were calculated.

(C) Quantification of protrusions per cell (means indicated). Representative Cav1WT and Cav1KO cells (asterisks mark protrusions) are shown.

(D) Cav1WT and KO MEFs were embedded (6 hr) in Col-I gels (1 mg/ml). EFs are indicated.

(E) Rac1 distribution in Cav1WT and KO MEFs. (a) Rac1 immunostaining in cells plated (4 hr) on FN. Asterisks mark Rac1 foci. (b) Rac1 pixel intensity from the cell edge to the nucleus. (c) Immunoblot showing total Rac1 expression.

(F) Gel contraction by Cav1WT and KO MEFs embedded in Col-I gels.

(G) Cav1-dependent cell elongation (a) and gel contraction (b) require Cav1-Tyr14.

Data are represented as mean ± standard error of the mean (SEM). See also Figure S1.

The level of Cav1WT FDM organization was consistent with published results for normal fibroblasts (Amatangelo et al., 2005). A similar level of parallelism was obtained in FDMs generated by Cav1KO MEFs re-expressing Cav1WT, but not Cav1Y14F (Figures 3C and 3D). Therefore, Cav1, via Tyr14, plays an important role in the topographical organization of 3D microenvironments.

Higher-than-normal parallelism is characteristic of tumor stromal collagen fibers and matrices generated by CAFs

(Amatangelo et al., 2005; Provenzano et al., 2008). Moreover, a stiff and ordered 3D microenvironment is essential for TC invasiveness, and highly aligned and organized collagen fibers increase matrix strength and stiffness in vivo (Gaggioli et al., 2007; Levental et al., 2009; Provenzano et al., 2008). Evaluation of FDM stiffness by atomic force microscopy (AFM) revealed that the Young Modulus of Cav1WT-derived FDM is 40% larger and has a wider standard deviation than that of Cav1KO FDM (Figure 3E and Figure S3A). Lack of Cav1 in MEFs thus makes the self-derived ECM less stiff and unifies its mechanical response. Cav1WT- and Cav1KO-derived FDMs were of equal thickness, and there were no significant differences in cell density before extraction (Figure S3B). Proteomic analysis revealed only slight, nonsignificant differences in the relative abundance of ECM proteins in WT and Cav1KO FDMs (Figure S3C).

Examination of tissue architecture in Cav1KO mice by Masson's trichrome and picrosirius red (PR) staining revealed a thicker and less organized collagen-rich dermis in both adult and young mice (Figure 3F and Figure S3D). We next used multiphoton excitation microscopy coupled to second harmomic generation (MPE-SHG) imaging to study tissue organization at the mammary gland epithelial-stroma interface. SHG signal intensity was higher in Cav1WT mammary glands, in both the gland vicinity (Figure 3G) and neighboring stroma (Figure S3E), indicating greater collagen fiber organization. Tissues also contained collagen fibers devoid of SHG signal, which were often kinked in Cav1KO mammary glands but almost all straight in Cav1WT (Figure 3Ga and Figure S3E). PR staining confirmed disturbed collagen fiber organization in Cav1KO mammary glands, highlighting deficiency in fibrillar collagen around the acinus (Figure 3Gb).

Cav1 Promotes Force-Dependent Remodeling of the Surrounding Environment via Rho GTPase Activation

FN fibrillogenesis relies on Rho GTPase-dependent cell contractility, which generates tensile forces that expose cryptic self-assembly sites in stretched FN molecules (Zhong et al., 1998). Although their fibrillogenesis was delayed, Cav1KO MEFs were able to remodel the FN coating at later time points (Figure S4A) with similar FN expression levels as Cav1WT MEFs (Figure S4B). Absence of Cav1 thus delays but does not negate FN remodeling. Re-expression of Cav1 in Cav1KO MEFs restored cell-mediated FN fibrillogenesis (Figure 4A); re-expression of Cav1Y14F had no effect (Figure S4C). Cav1 deficiency decreases Rho activity via the endogenous inhibitor p190 (Grande-Garcia et al., 2007). Constitutive activation of Rho GTPase in Cav1KO MEFs rescued the FN remodeling phenotype but had no effect on Cav1WT MEFs (Figure 4A). Defective FN remodeling in Cav1KO MEFs was also reversed by stable silencing of p190 (Figure 4B and Figure S4Da), which decreased Rac activity and PM localization (Figure 4C and Figure S4Db). p190 knockdown (KD) also increased pMLC levels (not shown) and rescued cell contractility (Figure 4D). Moreover, p190 KD in Cav1KO MEFs increased the parallel fiber organization of derived matrix (Figure 4E), and this matrix increased the EF and decreased the number of protrusions of seeded Cav1WT MEFs (Figure 4F). Off-target effects were excluded with additional shRNAs (Figures S4E and S4F).

p190 activation is associated with its phosphorylation and partitioning into PM-ordered domains, where it inhibits Rho activity (Mammoto et al., 2007a; Sordella et al., 2003). We reported mildly increased p190 expression and phosphorylation in the absence of Cav1 (Grande-Garcia et al., 2007). In contrast to Rac1 and pPAK, p190 PM targeting was independent of Cav1 expression (Figure 4G). However, p190 phosphorylation at the PM was higher in the absence of Cav1 (Figure 4H). Cav1 absence also promoted p190 partitioning into PM-ordered domains, an effect reversed by Cav1 re-expression (Figure 4I). Cav1 thus appears to remodel the 3D microenvironment by stimulating Rho-dependent cell contractility and to regulate Rho activity by controlling the phosphorylation and partitioning of p190 into membrane-ordered domains.

Stroma of Human Breast, Kidney, and Colon Carcinoma and Melanoma Metastases Are Enriched in Cav1-Expressing Fibroblasts

Fibroblasts generate and remodel the stroma surrounding tumors. Microenvironments generated by CAFs display Rho-dependent parallelism (Amatangelo et al., 2005; Provenzano et al., 2008), suggesting that stromal Cav1 and its remodeling activity might affect tumor progression. We therefore analyzed tumor-associated stroma of various carcinomas.

Because Cav1 expression modifies mammary tissue architecture, we immunostained for Cav1 and SMA in a tissue microarray of 132 primary breast tumors and 35 normal breast tissues, scoring specifically for expression level in fibroblastic stroma (Figures 5A–5D and Table S1). Expression levels of Cav1 and SMA were significantly higher in tumor stroma ($p < 0.0001$) and showed a mild statistical correlation ($r = 0.54$) (Figure 5B). Mean and median SMA values were marginally higher in high- than in low-stage disease (Wilcoxon $p = 0.064$). Moreover, Cox proportional hazards analysis showed that patients with stromal Cav1 expression had a 2.5 times higher 10 year mortality risk (Figures 5C and 5D). In vitro assessments showed that Cav1 expression was significantly higher in breast CAFs than in normal fibroblasts (NFs) (Figure 5E). Stromal Cav1 expression is thus a potential indicator of breast carcinoma progression.

Tissue sections from five patients with renal carcinoma showed high tumor stromal Cav1 expression localized to blood vessels and CAFs (Figure 5F and Figures S5A and S5B). In contrast, Cav1 expression was low in healthy tissue and was mostly restricted to blood vessels and glomerular tubules. Stromal Cav1 expression in tumor sections was accompanied by a clear stromal reaction shown by positive SMA staining and collagen deposition (Figure 5F and Figure S5A). Next, NFs and CAFs harvested from patient #2 (Cav1 homogeneously stained the tumor-associated stroma) were induced to secrete and organize their own 3D in vivo-like matrices. Three-dimensional CAF cultures showed strong Cav1 and characteristic myofibroblast SMA expression (Figure 5G). We tested the effect of Cav1 KD on the ability of CAFs to contract Col-I gels. Similar infection efficiencies were obtained, but Cav1 KD was more efficient in NFs (Figure 5H). As reported (Orimo et al., 2005), CAFs retracted Col-I gels more efficiently than NFs (Figure 5I). Mild Cav1 KD in CAFs was sufficient to decrease contraction to NF levels (Figure 5I). Similar results were obtained with a different

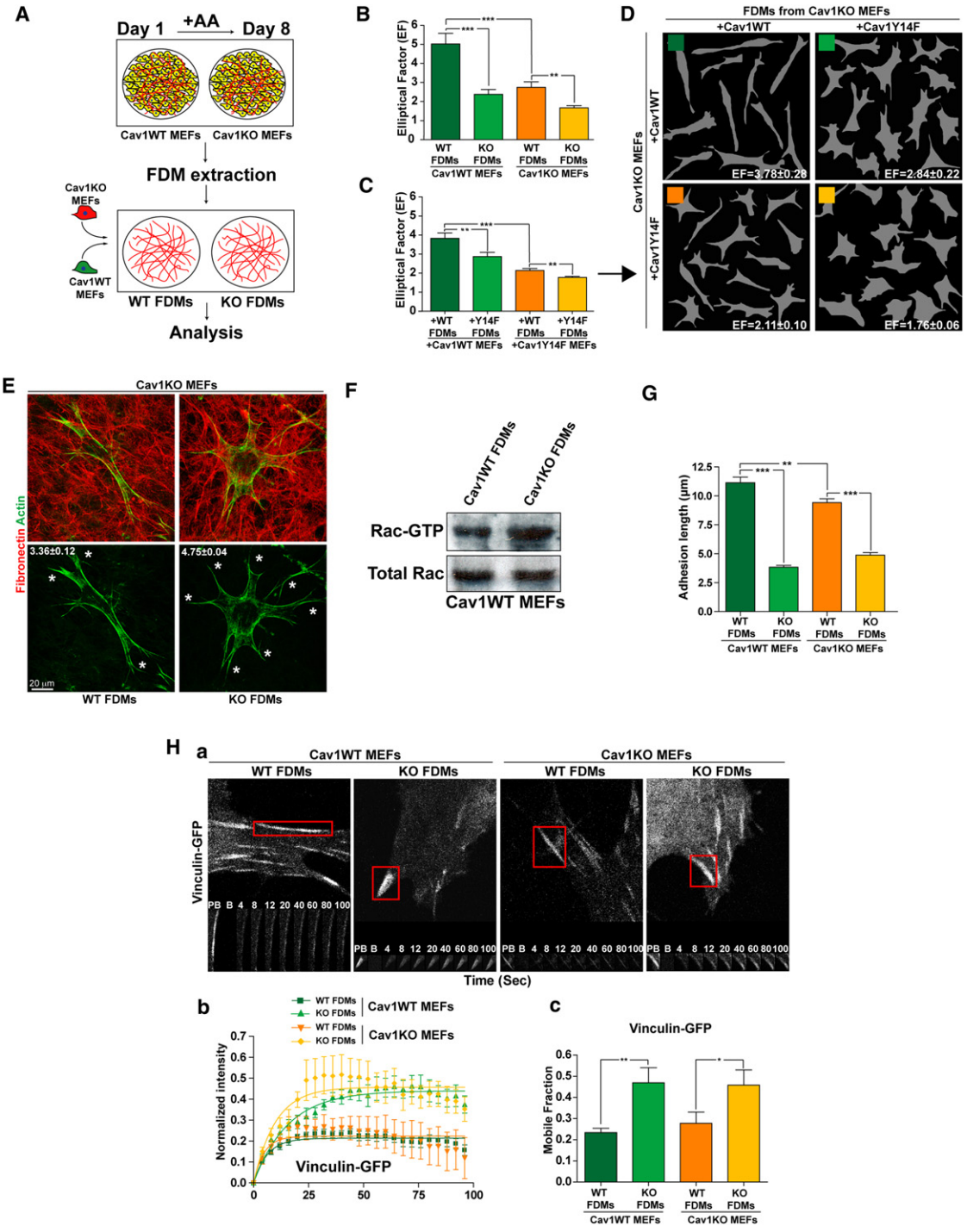

Figure 2. Cav1-Dependent Extracellular Environment Regulates Cell Shape, Protrusion Number, Rac1 Activity, and Maturation of Integrin-Dependent Adhesions

(A) FDMs were generated from Cav1WT and KO MEFs (or KO MEFs rescued with Cav1WT or CavY14F) and seeded with unmodified or reconstituted MEFs as indicated.

(B) EFs of Cav1WT and KO MEFs seeded in the indicated FDMs.

(C) EFs of Cav1KO MEFs rescued by re-expression (+) of Cav1WT or CavY14F and seeded in FDMs generated by similarly rescued Cav1KO MEFs.

(D) Representative Metamorph masks from experiments as in (C), with calculated EFs.

(E) Representative Cav1KO MEFS seeded in Cav1WT or Cav1KO FDMs; average protrusions per cell are shown.

(F) Rac-GTP levels and total Rac expression in Cav1WT MEFs seeded in Cav1WT or KO FDMs.

Cav1 siRNA (Figure S5C). Cav1 thus contributes to the contractile phenotype of CAFs, and its stromal expression might indicate renal carcinoma progression.

We next explored fibroblast Cav1 expression in colorectal cancer stroma, as this is one of the most common causes of cancer death in Western countries and its outcome is determined by the occurrence of metastatic dissemination. In normal tissue, Cav1 is expressed in smooth muscle cells of the muscularis mucosae, in blood vessels, and to a lower extent in the stroma underlying the epithelium (Figure 5J). Analysis of a tissue microarray of 84 colorectal carcinomas detected Cav1 expression in tumor-associated stroma but not in the epithelial TCs (~98% of cases). Cav1 staining intensity scores revealed strong expression in 75% of tumor-associated stroma (Figure 5J).

Cav1 was also expressed in the peritumoral stroma of all metastatic foci examined in a set of human melanoma metastatic explants, with >80% of fibroblasts being Cav1 positive (Figure 5K). Cav1 was found in 79% of fibroblasts expressing SMA and 82% expressing CD90, a marker of human CAFs (Figure 5K). Cav1 expression was detected in very few metastatic (Hmb-45$^+$) TCs and in only 36% of infiltrated (CD45$^+$) leukocytes (Figure 5K and Figure S5D). Cav1-expressing CAFs were excluded from tumor nests but were accompanied by heavy collagen and light FN deposits in the immediate peritumoral stroma (Figure S5E). Fibroblasts positive for CD90 and Cav1 were detected in distant tumor-associated stroma but were absent from normal connective or muscle tissue (not shown). Cav1 in nontumor tissue was localized exclusively in blood vessels. Stroma of metastatic foci is thus enriched in Cav1-positive CAFs, suggesting that stromal Cav1 might be instrumental in both primary and secondary tumor niches.

Cav1-Dependent 3D Microenvironment Stimulates In Vitro Tumor Cell Migration and Invasion

To investigate the mechanism by which microenvironment remodeling by stromal Cav1 affects TC behavior, we used three metastatic cell lines as representative models: MDA-MB-231 parental breast cancer cells (here called ATCC-231) and derived lines selected for in vivo tropism to lung (LM-4175) and bone (BM-1833) (Minn et al., 2005). All three lines express high levels of Cav1 (not shown). Metastatic cells seeded in FDMs generated by Cav1WT MEFs had a higher EF than when seeded in Cav1KO FDMs (Figure 6A). Cav1WT matrices also supported higher directionality and velocity of migration by TCs (Figure 6B, Movie S4, and Movie S5).

Although coculture with Cav1WT MEFs in Col-I gels only slightly increased TC EF (Figure S6A), it clearly favored TC invasion of the surrounding gel (Figure 6C and Figure S6C). Invading Cav1WT fibroblasts and TCs were both highly polarized and oriented perpendicular to the "tumor boundary" (Figure S6B). In an alternative matrigel-based 3D invasion assay, Cav1WT MEFs similarly promoted invasion by PC3 prostate TCs without displaying any differences in proliferation rate (Figure 6D and Figures S6C–S6E), suggesting that fibroblast Cav1 is a general promoter of TC invasion. In both models Cav1WT MEFs invaded significantly faster than Cav1KO MEFs and preceded TCs, as previously reported (Gaggioli et al., 2007). Similar results were obtained when fibroblasts were spatially separated from TCs by a thin matrigel layer in order to mimic tumor-stroma topography (Figure S6E). p190 KD in Cav1KO MEFs restored Cav1WT fibroblast-induced tumor cell invasiveness (Figure 6D and Figure S6C).

Cav1-Dependent 3D Microenvironment Stimulates In Vivo Tumor Cell Invasion and Increases Metastatic Potency

The contribution of fibroblastic Cav1 to stroma-dependent tumorigenesis in vivo was explored in a luminescence-based orthotopic mammary gland tumor formation assay, in which luminescent and GFP-expressing cells from mammary adenocarcinoma E0771 were injected into mammary glands of syngenic WT and Cav1KO mice (Figure 7A). Absence of host Cav1 slightly decreased primary mammary tumor growth (Figure 7Ab and Figure S7Aa) and metastasis formation (Figure S7Ab). No significant differences were observed when cells were injected in tail vein; in fact Cav1KOs appeared to have a slight advantage over WTs (Figure S7D). We next studied tissue architecture at the tumor-stroma interface by MPE-SHG. Tumors grown in Cav1KO mice were minimally invasive: TCs were localized in regions surrounded by few kinked and disorganized collagen fibers (Figures 7Ac and 7Ad). In contrast, tumors grown in Cav1WT mice were collagen-rich, with invading TCs in intimate contact with aligned straight and curly collagen fibers (Figures 7Ab and 7Ac). Consistent with proinvasion radial alignment of collagen fibers relative to tumor boundary (Provenzano et al., 2006), the angle of collagen fibers was significantly more perpendicular in WT than in Cav1KO hosts (Figure 7Ad), suggesting higher invasivity in WT environment.

Because Cav1 is implicated in tumor angiogenesis, vessel leakiness, and extravasation (Gratton et al., 2003), we conducted experiments to rule out effects derived from these actions. Orthotopic mammary gland tumors were obtained by injecting LM-4175 human TCs into lethally irradiated Cav1WT or Cav1KO mice (Figure 7B). After 9 days, equal-size tumors were either processed or transplanted together with their surrounding stroma into nude mice (Figure 7Ba). In this system, Cav1-dependent stroma is the only variable likely to affect TC invasiveness and metastatic potency. Using MPE-SHG imaging and histology, we evaluated Cav1-dependent matrix remodeling at the tumor-stroma interface of early tumors (8 days). Tumors grown in Cav1KO mice were minimally invasive. Collagen fibers were stretched and distributed tangentially along the tumor boundary, probably constraining tumor growth and consistent with previously described TACS-2 (Tumor-associated collagen

(G) Length of integrin-dependent adhesions (indicated by 9EG7 staining).

(H) FRAP analysis of vinculin-GFP-labeled adhesions in transfected cells seeded in the indicated FDMs. (a) Timelapse sequences showing corresponding regions before photobleaching (*PB*), immediately after photobleaching (*B*), and during recovery. (b) Quantification of vinculin-GFP fluorescence recovery for each condition. (c) Percentage of recovery (boxed areas in a) showing the size of the mobile vinculin-GFP fraction. Data are representative of three independent experiments ($6 \leq$ adhesions ≤ 15).

Data are represented as mean ± standard error of the mean (SEM). See also Figure S2.

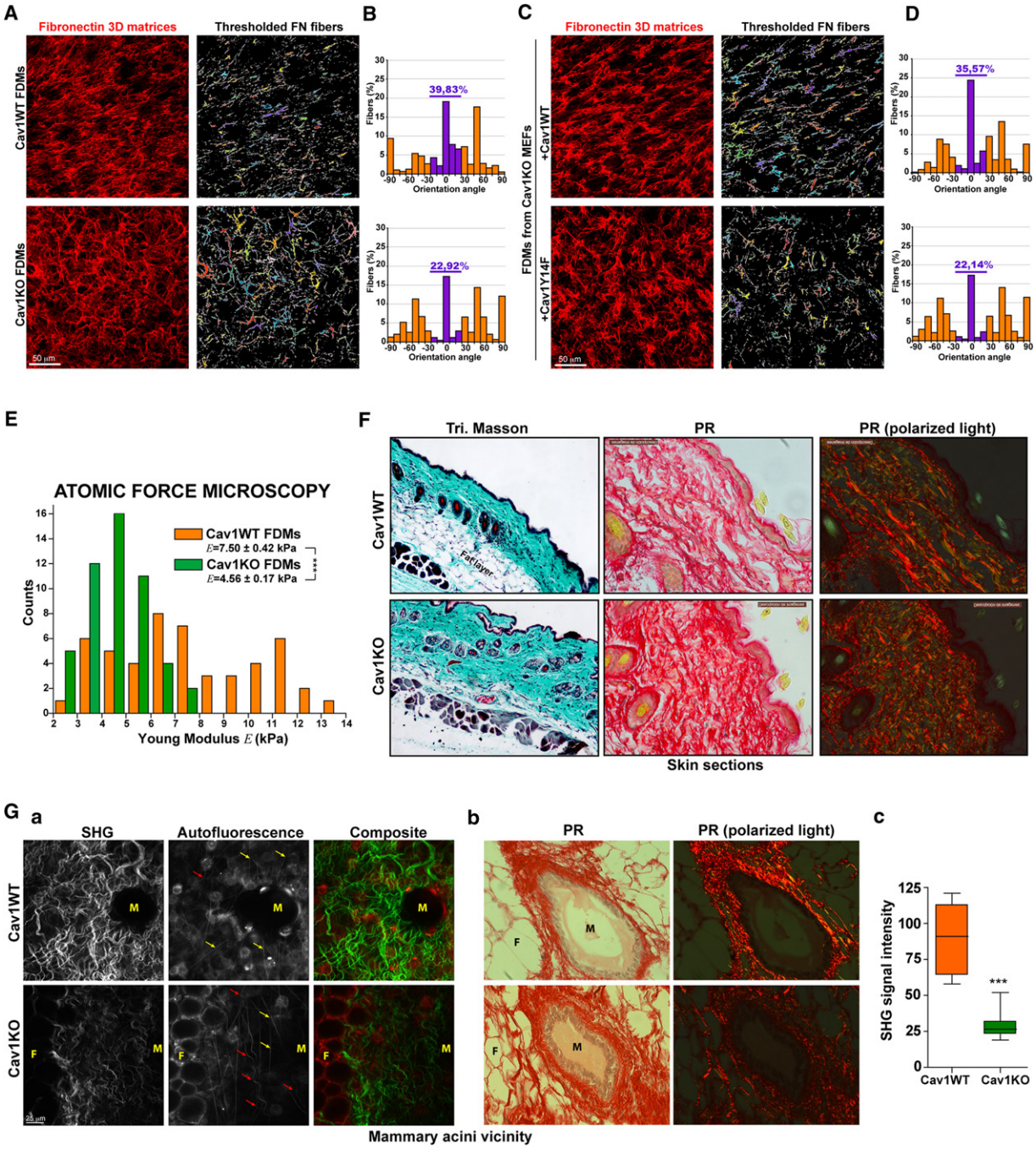

Figure 3. Cav1 Promotes Patterning and Stiffness of 3D Matrices and Favors Normal Tissue Architecture

(A–D) FDMs were generated and after cell extraction were fixed and labeled. The orientation of all thresholded FN fibers was quantified and plotted against the modal angle (set at 0°).

(E) Atomic force microscopy was used to plot point-by-point force versus distance along fibers. The chart shows quantification of Young modulus.

(F) Skin sections of WT and Cav1KO mice stained with Masson's trichrome and picrosirius red (PR). Polarized light highlights fibrillar collagen.

(G) Stromal organization in WT and Cav1KO mammary gland. (a) Multiphoton excitation microscopy coupled to second harmomic generation imaging (MPE-SHG) of intact fixed glands; SHG and autofluorescence signals are shown. Red and yellow arrows mark curled and straight collagen fibers devoid of SHG signal. (b) Mammary gland sections from WT and Cav1KO mice stained as in (F). M = mammary gland, F = fat cell. (c) Quantification of SHG signal intensity as in (a). Data are represented as mean ± standard error of the mean (SEM). See also Figure S3.

signature-2) (Provenzano et al., 2006) (Figures S7Ba and S7Bb). Indeed, tumors generated in Cav1KO mammary glands grew slower before (not shown) and after transplantation into nude mice (Figure S7Bc). In contrast, WT tumors had an invasive morphology, with both TCs and collagen fibers aligned in the direction of invasion (~90° to the tumor boundary), typical of TACS-3. After transplant, such tumors generated significantly more metastases in most organs analyzed (Figure 7Bb). These tumors moreover displayed significantly increased matrix fiber parallelism and alignment, and elongation of SMA-positive CAFs (Figures 7Bc and 7Bd and Figure S7Bd). Interestingly, alignment of intratumoral FN fibers correlated with the number of metastasis (n = 10, Figure 7Bd). These results indicate that Cav1-positive surrounding stroma regulates primary tumor growth and favors invasion and metastasis.

Because Cav1 was absent in all tissues, neither of the approaches described tests the effect of specific lack of Cav1 in the tumoral stroma associated with the orthotopic xenograft. To overcome this and to test the role of p190 in metastatic potency in vivo, we designed a luminescence-based subcutaneous tumor formation assay in which Matrigel-embedded luminescent TCs (LM-4175) were mixed with pMEFs (Cav1WT, Cav1KO, or p190-silenced Cav1KO pMEFs) (Figure 7Ca) and injected subcutaneously into nude nice (Figure 7C). The microenvironment-remodeling properties of pMEFs are similar to those of their immortalized counterparts (not shown). p190 was stably silenced in Cav1KO pMEFs and Cav1 was expressed only in Cav1WT pMEFs (Figure 7Ca). There was no difference in primary tumor growth (Figure S7Ca and Figure 7Cc); but Cav1WT pMEFs were more potent stimulators of metastasis formation than Cav1KO pMEFs (Figures 7Cb and 7Cc), confirming the results obtained in orthotopic mammary assays and validating this assay for studying the mechanism of stroma-dependent tumor invasion and metastasis. Deficiency in metastasis deposition was rescued by p190 KD in Cav1KO pMEFs (Figures 7Cb–7Cd). Study of intratumoral stroma remodeling in tumor explants revealed an increase in FN fiber alignment when injected pMEFs expressed Cav1. Deficient alignment was rescued by p190 KD in Cav1KO MEFs (Figure 7Cc and Figures S7Cb and S7Cc). Intratumoral FN fiber alignment and metastatic potency were statistically correlated (n = 30, Figure 7Cd). Additionally, rescue of normal Rho activity (in p190-silenced Cav1KO pMEFs) increased alignment and elongation of SMA-positive fibroblasts (Figure S7Cb).

Together these results demonstrate that stromal Cav1, through p190-dependent regulation of Rho-mediated cell contractility, remodels peri- and intratumoral microenvironments to facilitate TC invasion and metastasis. These data identify an important role for stromal-expressed Cav1 in tumor progression, consistent with the human tumor histology data, and highlight the importance of mechanical remodeling of the microenvironment in tumor metastatic potency.

DISCUSSION

Our results show that intrinsic fibroblast Cav1 and the Cav1-regulated microenvironment cooperate to enhance cell elongation, migration, and invasion through force-dependent organization of the surrounding 3D environment. Cav1 mediates these effects by regulating Rho activity via changes in p190 localization and phosphorylation. Our data suggest that this Cav1-dependent bidirectional cell/matrix mechanical crosstalk is critical for normal tissue homeostasis and architecture and for tumor invasion and metastasis.

Cav1 in Tumor-Associated Stroma

Our study identifies Cav1 as a regulator of ECM remodeling and desmoplastic processes. CAFs, the main cell component of the desmoplastic stroma of solid cancers and their metastases (Bhowmick et al., 2004), influence TC growth through paracrine secretion of growth factors and recruit endothelial progenitors to promote angiogenesis (Karnoub et al., 2007; Orimo et al., 2005). CAFs deposit ECM and remodel the tumor stroma. ECM fiber tracks align at the tumor margin, and force- and protease-mediated ECM remodeling by fibroblasts favors TC invasion (Gaggioli et al., 2007; Provenzano et al., 2006, 2008). Here we show that the stroma of breast, renal, and colon carcinoma and melanoma metastases is enriched in Cav1-expressing CAFs, and contractility of renal CAFs is reduced by lowering Cav1 levels. Cell-free 3D matrices generated by Cav1WT fibroblasts are stiffer and more aligned than matrices derived from Cav1KO fibroblast, thus better stimulating TC elongation, velocity, and directional migration. Orthotopic implantation in Cav1KO mice impairs tumor invasiveness and metastatic potency. In cocultures fibroblast Cav1 favors TC invasion, and coinjection of these cells into nude mice increases metastasis. Both effects depend on Cav1-regulated p190 activity. Results from the experimental metastasis assay suggest an important role of fibroblast Cav1 in events before intravasation. Thus CAF expression of Cav1 favors tumor progression via biomechanical remodeling of the primary tumor-associated stroma. These findings may help explain the somewhat contentious role of Cav1 in tumorigenesis, as the protumorigenic action of Cav1 may depend on expression by stromal fibroblasts.

Our results indicate that evaluation of tumorigenic potential requires examination of both tumor and stroma, especially for Cav1 expression. Cav1 was enriched in the stroma of various tumors, and stromal Cav1 was linked to poor survival. We found a positive correlation between Cav1 and the CAF marker SMA, similar to that described in pancreatic cancer (Witkiewicz et al., 2008). This appears to conflict with reports proposing stromal Cav1 expression as a positive prognostic indicator in breast cancer; however, these studies did not link Cav1 expression to a positive CAF marker, and loss of stromal Cav1 did not correlate with metastasis (Sloan et al., 2009; Witkiewicz et al., 2009). Cav1 thus appears to have a complex role in tumor stroma, and further work is needed to justify the potential use of Cav1 for prognosis. Our findings with orthotopic grafts and the stroma-dependent tumorigenicity assay suggest that increased fibroblast Cav1 would promote local invasiveness and metastasis via remodeling of the stromal ECM. Cav1 could also regulate other (nonfibroblast) tumor-associated stromal components.

Stromal Cav1 in Normal and Pathological Tissue Architecture

Through reciprocal cell–ECM interactions, the stroma provides environmental cues essential for tissue architecture. The ability

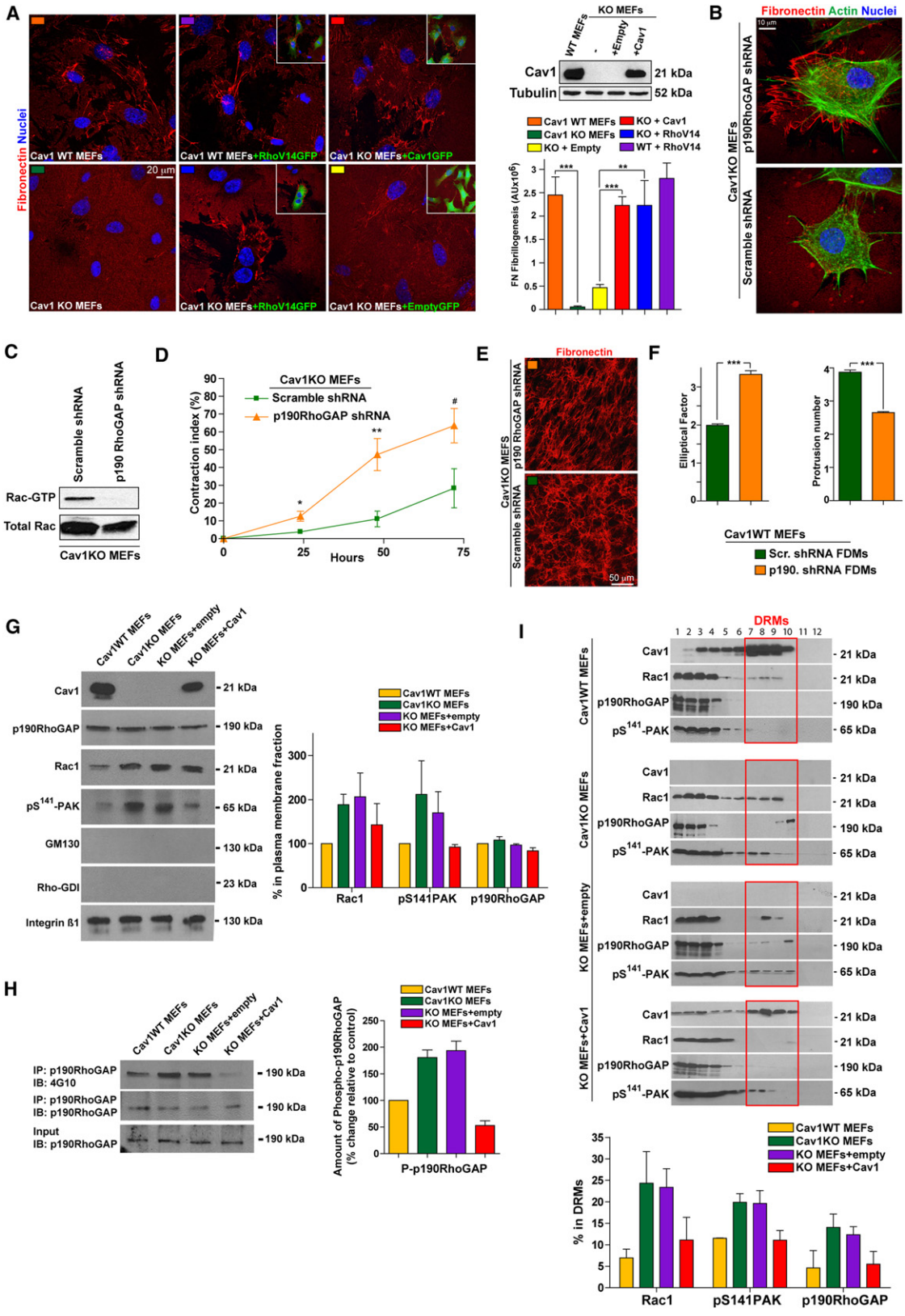
A
Fibronectin Nuclei
Cav1 WT MEFs
Cav1 WT MEFs+RhoV14GFP
Cav1 KO MEFs+Cav1GFP
20 μm
Cav1 KO MEFs
Cav1 KO MEFs+RhoV14GFP
Cav1 KO MEFs+EmptyGFP
KO MEFs
WT MEFs
-
+Empty
+Cav1
Cav1
21 kDa
Tubulin
52 kDa
Cav1 WT MEFs
Cav1 KO MEFs
KO + Empty
KO + Cav1
KO + RhoV14
WT + RhoV14
FN Fibrillogenesis (AUx10^6)
B
Fibronectin Actin Nuclei
10 μm
Cav1KO MEFs
p190RhoGAP shRNA
Scramble shRNA
C
Scramble shRNA
p190 RhoGAP shRNA
Rac-GTP
Total Rac
Cav1KO MEFs
D
Cav1KO MEFs
Scramble shRNA
p190RhoGAP shRNA
Contraction index (%)
Hours
E
Fibronectin
Cav1KO MEFS
p190 RhoGAP shRNA
Scramble shRNA
50 μm
F
Elliptical Factor
Protrusion number
Cav1WT MEFs
Scr. shRNA FDMs
p190. shRNA FDMs
G
Cav1WT MEFs
Cav1KO MEFs
KO MEFs+empty
KO MEFs+Cav1
Cav1
p190RhoGAP
Rac1
pS141-PAK
GM130
Rho-GDI
Integrin ß1
21 kDa
190 kDa
21 kDa
65 kDa
130 kDa
23 kDa
130 kDa
% in plasma membrane fraction
Rac1
pS141PAK
p190RhoGAP
H
IP: p190RhoGAP
IB: 4G10
IP: p190RhoGAP
IB: p190RhoGAP
Input
IB: p190RhoGAP
190 kDa
Amount of Phospho-p190RhoGAP (% change relative to control)
P-p190RhoGAP
I
DRMs
1 2 3 4 5 6 7 8 9 10 11 12
Cav1WT MEFs
Cav1KO MEFs
KO MEFs+empty
KO MEFs+Cav1
Cav1
Rac1
p190RhoGAP
pS141-PAK
21 kDa
21 kDa
190 kDa
65 kDa
% in DRMs
Rac1
pS141PAK
p190RhoGAP

of fibroblast-Cav1 to modulate cell morphology via force-dependent ECM remodeling suggests that its absence could disturb normal tissue architecture. Consistently, Cav1 loss in stromal cells produces benign stromal lesions causing abnormal epithelium growth and differentiation (Yang et al., 2008). Disturbed fibroblast function might underlie pulmonary fibrosis, hypertension, and cardiac fibrosis and hypertrophy in Cav1KO mice (Drab, 2001; Razani et al., 2001; Zhao et al., 2002). The observed overproduction of disorganized fibrous connective tissue in Cav1KO mice might be responsible for delayed wound healing in Cav1KO mice (Grande-Garcia et al., 2007). We also report that Cav1WT mammary glands show markedly higher SHG signal intensity and numbers of straight collagen fibers. Disorganization of collagen-rich mammary stroma in Cav1KO mice could account for mammary dysplasia and ductal thickening (Williams et al., 2006). The correlation between disorganized mammary stroma and impaired growth, invasion, and metastatic potency of orthotopic grafts suggests that Cav1-positive stroma is permissive for tumor progression, consistent with retarded growth of subcutaneous grafts in Cav1KO mice (Chang et al., 2009). Together, this suggests that Cav1-dependent impaired architecture of native stroma might also affect tumor progression.

Concerted Regulation of Cell Shape by Cav1-Dependent Microenvironment and Endogenously Expressed Cav1

The FDMs generated in our study model the physiological microenvironment of cell interactions and reveal that the matrix generated by Cav1 fibroblasts increases cell elongation. Morphology of all cells tested was more strongly influenced by the surrounding 3D architectural organization than by its "intrinsic" shape in 2D. Earlier in vitro 2D studies showed that Cav1 phosphorylation at Tyr14 coordinates Rho GTPase activity (Grande-Garcia et al., 2007). We now show that Cav1 regulates p190 phosphorylation and partitioning into ordered domains, where it is known to inhibit Rho (Mammoto et al., 2007a; Sordella et al., 2003). Cav1 regulates Rac-binding sites in ordered domains (del Pozo et al., 2005), and we now show that lack of Cav1 generates Rac accummulation in these sites and could thereby mediate p190 recruitment (Bustos et al., 2008; Mammoto et al., 2007b). The Cav1-dependent 3D microenvironment cooperates with intrinsic Cav1 to enhance cell elongation by reducing Rac activity and the number of protrusions. Cav1-dependent Rho activity also potentiates the force-dependent ability of fibroblasts to contract the surrounding matrix. Increased matrix contractility is linked to elevated pMLC (Gaggioli et al., 2007), which is consistent with p190-dependent pMLC expression and contractility of Cav1-expressing cells, favoring microenvironment-dependent cell elongation. Fibroblast contractility is linked to SMA expression (Hinz, 2010), and SMA levels are increased in Cav1WT MEFs grown in 3D. Interestingly, force, via Rho/Rhokinase, promotes activation of the SMA promoter (Zhao et al., 2007), suggesting that Cav1-mediated increased rigidity of WT FDMs might promote SMA expression.

Cav1 and Microenvironment Anisotropy

Contact guidance implies that structural organization of ECM provides directional cues to cells and directs morphology and motility via anisotropy of the microenvironment (Doyle et al., 2009). Thus, intrinsic cell properties and the surrounding microenvironment can both drive cell behavior. Our results show that Cav1-expressing fibroblasts increase alignment of ECM fibers through Rho- and force-dependent matrix reorganization. In turn these matrices enhance cell elongation, mature integrin adhesions, and reduce cell protrusions. Contact guidance also occurs at the tumor-stroma interface, where disregulation generates a more parallel than normal matrix, guiding local invasion (Gaggioli et al., 2007; Provenzano et al., 2006, 2008). Our finding that tumor cell elongation, velocity, and migration directionality are enhanced by Cav1 FDMs is relevant here. Coculture with Cav1 fibroblasts favors TC elongation and invasiveness in vivo and in vitro. The tumor-stroma interface of mammary tumors in Cav1-expressing mice is more proinvasive than in their Cav1KO counterparts, with increased collagen fiber alignment. Recent reports propose quantification of collagen alignment at the tumor boundary as a predictor of breast cancer survival (Conklin et al., 2011). We observed a strong correlation between metastatic potency and intratumoral matrix alignment, which might be used as a prognostic marker of carcinoma progression. Our findings may also be related to the increased Cav1 expression in metastatic lesions (Goetz et al., 2008b), where mesenchymal Cav1 might be required to produce an invasion-permissive environment and parenchymal Cav1 might promote directional migration and invasion.

Cav1 and Matrix Stiffness

Matrix stiffness disrupts tissue morphogenesis (Paszek et al., 2005), drives differentiation of mesenchymal stem cells (Engler et al., 2006), and fosters tumor progression (Levental et al., 2009). Rho-dependent cell contractility is also closely related to matrix stiffness and orientation (Paszek et al., 2005; Provenzano et al., 2008). The ability of AFM to probe mechanical properties of synthetic, near-physiological matrices is well-established (Engler et al., 2006) but had not been applied before

Figure 4. Cav1 Promotes Force-Dependent Microenvironment Remodeling via Rho GTPase Activation

(A) Indicated MEFs expressing GFP-tagged WT Cav1, RhoV14, or empty vector (see immunoblot) were plated on FN (24 hr). FN remodeling was quantified by thresholding for bright FN fibrils.

(B) Cav1KO MEFs stably expressing scrambled or p190 shRNA were plated as in (A) and analyzed for (C) Rac1-GTPase activity and (D) Col-I gel contraction.

(E) FN staining of FDMs generated from the indicated MEFs.

(F) EF (left) and average protrusion number (right) of Cav1WT MEFs seeded on FDMs generated as in (E).

(G) Immunoblot analysis of purified PM fractions from the indicated MEFs. Quantified and protein levels are plotted relative to Cav1WT MEFs.

(H) p190 was immunoprecipitated from samples prepared as in (G) and probed for p190 and phosphotyrosine (4G10). Chart shows quantification of phosphorylated p190.

(I) The indicated MEFs were fractioned, and immunoblot signals in DRM fractions quantified and plotted.

Data are represented as mean ± standard error of the mean (SEM). See also Figure S4.

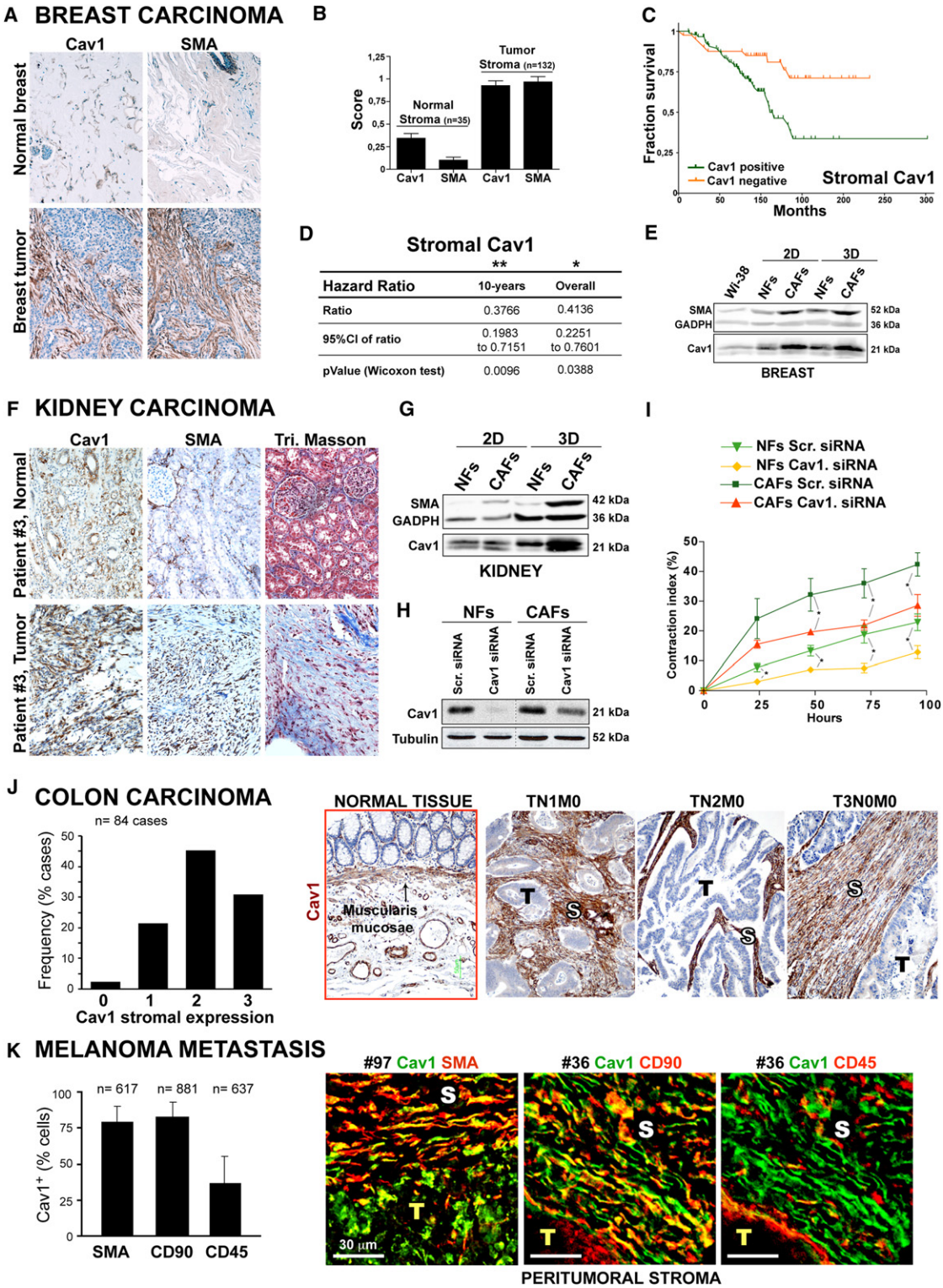

Figure 5. Stroma of Human Breast, Kidney, and Colon Carcinomas and Melanoma Metastases Are Enriched in Cav1-Expressing Fibroblasts

(A) Representative images of normal and breast cancer tissue stained for Cav1 and SMA.

(B) Staining scores for Cav1 and SMA in normal (n = 35) and tumor (n = 132) tissues.

(C) Kaplan-meier curve of progression-free survival for patients sorted by stromal Cav1 expression.

(D) Multivariate survival results for Cav1-positive and -negative stroma.

to FDMs. Our AFM studies revealed 40% higher rigidity in FDMs produced by Cav1 cells. Because no major difference was observed in ECM protein content between Cav1WT and Cav1KO FDMs, ECM remodeling or crosslinking might be solely responsible for the observed differential rigidity. Artificial increase of fibroblast-dependent collagen crosslinking in mouse mammary stroma stiffens the tissue and promotes growth and invasion by normally noninvasive mammary epithelial cells (Levental et al., 2009). Together these findings suggest that the impact of Cav1 on directional TC invasion results from increases in ECM anisotropy and stiffness.

A growing body of work suggests that environment remodeling is essential for normal tissue architecture and for tumor progression. Our study identifies a critical role for Cav1 in these processes, highlighting a function of Cav1 in the regulation of matrix-dependent cell behavior. Elucidation of further proteins and mechanisms responsible for this function will provide fertile ground for future research.

EXPERIMENTAL PROCEDURES

Antibodies and Reagents

Ascorbic acid, ammonium hydroxide, and Triton X-100 were from Sigma. Primary antibodies: Rac and p190RhoGAP (Upstate Biotechnology); RhoGDI (Santa Cruz), Cav1, CD90, GM130, CD45, and activated β1-integrin (9EG7) (BD); γ-tubulin, SMA, FN, and Col-I (Sigma); Hmb45 (Dako), pY397FAK, and PAK1/2/3[pS141] (Biosource); GADPH and 4G10 (Millipore). Secondary antibodies were from Molecular Probes and from Jackson. FN was purified from human plasma.

Cell Culture

pMEFs and 3T3-immortalized MEFs from WT and Cav1KO mice were cultured as described (Cerezo et al., 2009). ATCC-231, LM-4175, and BM-1833 were cultured as described (Minn et al., 2005). PC3 and E0771 TCs were cultured as recommended.

Mice

Cav1-deficient mice (STOCK Cav1^{tm1Mls}/J; Razani et al., 2001) and WT B6129SF2/J controls were from The Jackson Laboratory (USA). Cav1-deficient mice and WT littermates (B6.Cg-CAV1^{tm1mls}/J; Drab, 2001) were used for in vivo experiments. Female athymic nude mice were obtained from Harlan.

3D Cell Culture and Assays

FDM production and the Matrigel-invasion assay are described in the Extended Experimental Procedures. The spheroid invasion assay was adapted from Gaggioli et al. (2007). After 6 days, invaded gels were fixed, labeled with fluorescently conjugated phalloidin, imaged, and analyzed. Invasiveness was quantified as the area invaded by tumor cells.

Col-I gel contraction assays were performed as published (Orimo et al., 2005). Four or five fibroblast-containing gels were assayed for each condition. Gel contraction index was calculated with Metamorph software from the gel surface area measured on acquired images and reported as the percentage of contraction of the initial surface area.

Tumorigenicity Assays and Bioluminescent Imaging

Mammary gland grafts and experimental metastasis assays are described in the Extended Experimental Procedures. Alternatively, LM-4175, alone or mixed with pMEFs, was subcutaneously injected following Karnoub et al. (2007). Tumor growth and metastasis were assessed by bioluminescence with the IVIS Imaging System. Briefly, mice were injected with luciferin (17.5 mg/ml) and after 20 min were placed in the IVIS Imaging System and ventral views captured. Tumor growth and metastasis formation were monitored at regular intervals. Exposure time for photon flux quantification was 0.2 s but ranged from 0.2 s to 2 min for metastasis detection. At the end of the in vivo analysis, luciferin-injected mice were killed and the organs extracted and reimaged ex vivo to detect metastatic foci. Images acquired from multiple exposure times were used to manually quantify every visible metastatic focus. Small metastatic foci could be detected by adjusting the scale of photon flux in Living Image 3.2. Extracted primary tumors were frozen in tissue-Tec and prepared for histology. Alternatively, tumor architecture was analyzed by SHG imaging.

Image Analysis of Immunofluorescence-Labeled Cells and Matrices

Images were captured with Leica confocal microscopes. EF was determined with MetaMorph (Universal Imaging Corp).

RNA Interference

Silencing of p190 was as described in (Grande-Garcia et al., 2007). Cav1 siRNA was as described (Gonzalez-Munoz et al., 2009). Alternative Cav1-siRNA sequences are shown in the Extended Experimental Procedures.

Liquid Chromatography and Tandem Mass Spectrometry

FDMs were extracted, labeled with iTRAQ reagents, and identified by LC-MS/MS as described in the Extended Experimental Procedures.

Microscopy Techniques

For 3D timelapse video microscopy, cells were seeded in FDMs and imaged for 12 hr (Movie S4 and Movie S5). Centroids were tracked with MetaMorph. Fluorescence recovery after photobleaching was performed as described (Goetz et al., 2008a). MPE-SHG imaging on formalin-fixed, intact, non-stained mammary glands and mammary tumors was as described (Provenzano et al., 2006). AFM is described in the Extended Experimental Procedures.

Tissue Samples, Cell Isolation, and Tumor Microarrays

Primary fibroblasts from paired normal human kidney and tumor samples and breast tumor microarrays (TMAs) were obtained from Fox Chase Cancer Center's Biosample Repository (Philadephia, PA, USA). Samples were blindly scored by a certified pathologist. Colon carcinoma and normal colon tissues were from the Centro Nacional de Investigaciones Oncológicas, Madrid, Spain. Human melanoma tissue was taken with informed consent from patients undergoing surgery at the Hospital Gregorio Marañón, Madrid. Tissue processing is described in the Extended Experimental Procedures.

(E) Fibroblasts from normal breast tissue (NFs) and tumor tissue (CAFs) were isolated and cultured as indicated. Immunoblot shows Cav1 and SMA expression.
(F) Paired sections of normal kidney and renal tumor tissue stained for Cav1 and SMA. Collagen deposition was assessed by Masson's trichrome staining.
(G) NFs and CAFs from normal kidney and renal tumor tissue of the same patient were isolated, cultured as indicated, and Cav1 and SMA expression was assessed.
(H) NFs and CAFs were infected with lentivirus expressing scrambled or Cav1 siRNA and Cav1 expression assessed.
(I) Col-I gel contraction by NFs and CAFs infected as in (H).
(J) Sections of normal colon and colorectal tumor tissue from 84 patients were stained for Cav1. Images are representative of control tissue and colorectal carcinoma with strong stromal Cav1. S = stroma, T = tumor. Chart shows percentage of cases classified according to Cav1 intensity from 0 = low (control tissue) to 3 = strong.
(K) Cav1, SMA, CD90, and CD45 expression in melanoma metastases. Images show colocalization analysis of Cav1 with SMA, CD90, and CD45.
Data are represented as mean ± standard error of the mean (SEM). See also Figure S5.

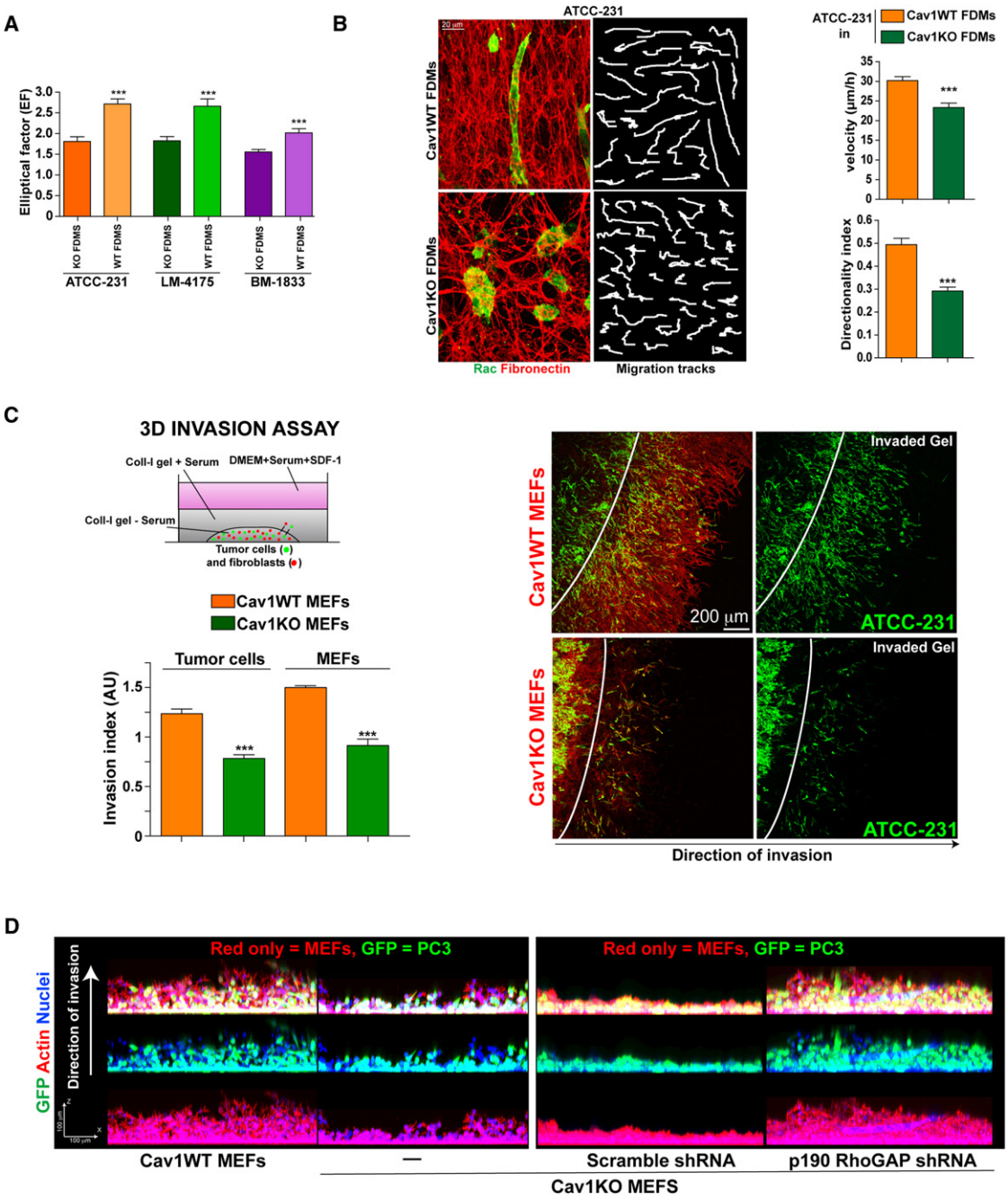

Figure 6. Cav1-Dependent 3D Microenvironment Stimulates TC Migration and Invasion In Vitro

(A) EFs of ATCC-231, LM-4175, and BM-1833 metastatic cells seeded in Cav1WT or Cav1KO FDMs.

(B) ATCC-231 cells grown in the indicated FDMs (6 hr) were monitored for 12 hr. Samples were labeled for Rac and FN to reveal cell morphology and FDM structure. Example migration tracks are depicted. Charts show quantification of cell velocity and directionality. See corresponding Movie S4 and Movie S5.

(C) Col-I gels containing prelabeled TCs and MEFs were placed under cell-free gel (scheme) and 3D TC invasion was quantified. Actin staining (red) allowed distinction of MEFs (red only) from TCs (green).

(D) GFP-expressing PC3 prostate TCs were seeded in Matrigel with the indicated MEFs and cultured for 6 days. Cells were fixed and stained as indicated. Data are represented as mean ± standard error of the mean (SEM). See also Figure S6.

Membrane Fractionation

Detergent-resistant and PM fractions were purified by standard procedures. p190 immunoprecipitation and biochemistry are described in the Extended Experimental Procedures.

Statistics

Error bars depict standard error of the mean (SEM). Statistical significance was determined with GraphPad Prism by unpaired Student's t test or Mann-Whitney test as indicated; * $p < 0.05$, ** $p < 0.01$, *** $p < 0.001$.

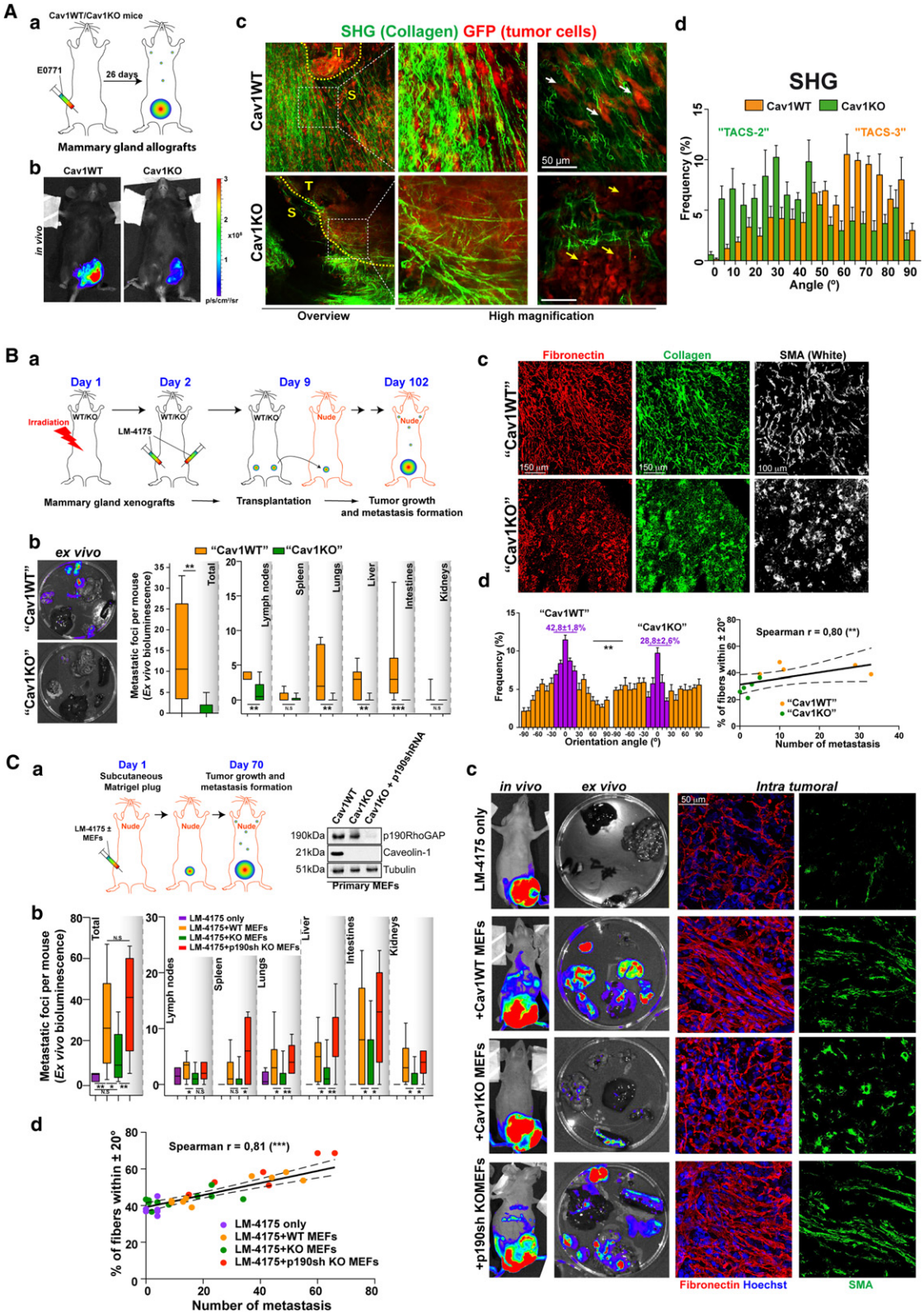
A
a
Cav1WT/Cav1KO mice
E0771
26 days
Mammary gland allografts
b
Cav1WT
Cav1KO
in vivo
p/s/cm²/sr
c
SHG (Collagen) GFP (tumor cells)
Cav1WT
Cav1KO
T
S
50 µm
Overview
High magnification
d
SHG
Cav1WT
Cav1KO
"TACS-2"
"TACS-3"
Frequency (%)
Angle (°)
B
a
Day 1
Day 2
Day 9
Day 102
Irradiation
WT/KO
LM-4175
Nude
Mammary gland xenografts
Transplantation
Tumor growth and metastasis formation
b
ex vivo
"Cav1WT"
"Cav1KO"
Metastatic foci per mouse (Ex vivo bioluminescence)
Total
Lymph nodes
Spleen
Lungs
Liver
Intestines
Kidneys
c
Fibronectin
Collagen
SMA (White)
"Cav1WT"
"Cav1KO"
150 µm
100 µm
d
"Cav1WT"
42,8±1,8%
"Cav1KO"
28,8±2,6%
Frequency (%)
Orientation angle (°)
Spearman r = 0,80 (**)
% of fibers within ± 20°
Number of metastasis
C
a
Day 1
Subcutaneous Matrigel plug
Day 70
Tumor growth and metastasis formation
LM-4175 ± MEFs
Nude
Cav1WT
Cav1KO
Cav1KO + p190shRNA
190kDa
21kDa
51kDa
p190RhoGAP
Caveolin-1
Tubulin
Primary MEFs
b
Metastatic foci per mouse (Ex vivo bioluminescence)
LM-4175 only
LM-4175+WT MEFs
LM-4175+KO MEFs
LM-4175+p190sh KO MEFs
Total
Lymph nodes
Spleen
Lungs
Liver
Intestines
Kidneys
N.S
d
Spearman r = 0,81 (***)
% of fibers within ± 20°
Number of metastasis
LM-4175 only
LM-4175+WT MEFs
LM-4175+KO MEFs
LM-4175+p190sh KO MEFs
c
in vivo
ex vivo
Intra tumoral
LM-4175 only
+Cav1WT MEFs
+Cav1KO MEFs
+p190sh KOMEFs
50 µm
Fibronectin Hoechst
SMA

SUPPLEMENTAL INFORMATION

Supplemental Information includes Extended Experimental Procedures, seven figures, one table, and five movies and can be found with this article online at doi:10.1016/j.cell.2011.05.040.

ACKNOWLEDGMENTS

We thank J. Massagué and R. Gomis for luciferase-expressing TCs; F. Sirotnak, M. Kolonin, and A. Schrum for E0771 cells; M. Morente, the CNIO Tumor Bank, and the Spanish National Tumor Bank Network for colon carcinoma TMA; the CNIC Viral Vector Unit for lentivirus; P. Martin and R. Mota for intravenous injection; I. Treviño for help with immunohistochemistry; K. Devarajan for breast TMA statistical analysis; V. Gupta, R. Castello-Cros, and D. Bassi for renal and breast CAF harvesting and immunohistochemistry; A. Alfranca for luciferase vector and advice; M. Montoya for advice on SHG and helpful discussion; F. Sanchez-Cabo for help with statistical analysis; A.U. for brainstorming; X. Bustelo, I.R. Nabi, G. Scita, and P.P. di Fiore for critical reading of the manuscript; and S. Bartlett for editing. This work was supported by grants from the MICINN (Spanish Ministry of Science and Innovation) to M.A.D.P. (SAF2008-02100, RTICC RD06/0020/1033, and CSD2009-00016), P.S.-M. (SAF2010-1602), and R.G. (MAT2009-08650 and CSD2010-00024); by EMBO Young Investigator Programme to M.A.D.P., and by the European Heads of Research Councils and the ESF through a European Young Investigator (EURYI) award to M.A.D.P.; and by NIH/NCI CA113451 and FCCC Kidney Keystone Program grants to E.C. J.G.G. and T.P. are CNIC postdoctoral fellows. S.M. and A.E. are *Ramón y Cajal* fellows. A.C. is a AECC (Spanish Association against Cancer) fellow. The CNIC is supported by the MICINN and the Pro-CNIC Foundation.

J.G.G. and M.A.D.P. designed the study and wrote the paper with input from E. Cukierman and S.M.; J.G.G. performed experiments and analyzed data; M.A.D.P. conceived the project, analyzed data, and directed the study. S.M. contributed to the design of in vivo experiments and conducted and analyzed experiments; I.N.-L. did the biochemistry experiments and cloning; J.J.L. and A.C. performed mouse experiments; R.S. and P.S.-M. analyzed melanoma, colocarcinoma, and mouse grafts; E. Calvo did proteomic analysis; M.T. and R.G. did AFM studies; T.O.-I. contributed technically to various experiments; T.P. performed the matrigel invasion assay; A.E. did cloning; A.J.P.K.-S. analyzed breast TMA; P.J.K. did 2HG analysis; E. Cukierman provided and analyzed kidney and breast CAFs and TMA. E. Cukierman, S.M., R.S., R.G., P.J.K., and P.S.-M. also provided intellectual insight.

Received: April 8, 2010
Revised: December 10, 2010
Accepted: May 31, 2011
Published: July 7, 2011

REFERENCES

Amatangelo, M.D., Bassi, D.E., Klein-Szanto, A.J., and Cukierman, E. (2005). Stroma-derived three-dimensional matrices are necessary and sufficient to promote desmoplastic differentiation of normal fibroblasts. Am. J. Pathol. *167*, 475–488.

Bershadsky, A.D., Balaban, N.Q., and Geiger, B. (2003). Adhesion-dependent cell mechanosensitivity. Annu. Rev. Cell Dev. Biol. *19*, 677–695.

Bhowmick, N.A., Neilson, E.G., and Moses, H.L. (2004). Stromal fibroblasts in cancer initiation and progression. Nature *432*, 332–337.

Bustos, R.I., Forget, M.A., Settleman, J.E., and Hansen, S.H. (2008). Coordination of Rho and Rac GTPase function via p190B RhoGAP. Curr. Biol. *18*, 1606–1611.

Cerezo, A., Guadamillas, M.C., Goetz, J.G., Sanchez-Perales, S., Klein, E., Assoian, R.K., and Del Pozo, M.A. (2009). Absence of caveolin-1 increases proliferation and anchorage-independent growth by a Rac-dependent, Erk-independent mechanism. Mol. Cell. Biol. *29*, 5046–5059.

Chang, S.H., Feng, D., Nagy, J.A., Sciuto, T.E., Dvorak, A.M., and Dvorak, H.F. (2009). Vascular permeability and pathological angiogenesis in caveolin-1-null mice. Am. J. Pathol. *175*, 1768–1776.

Conklin, M.W., Eickhoff, J.C., Riching, K.M., Pehlke, C.A., Eliceiri, K.W., Provenzano, P.P., Friedl, A., and Keely, P.J. (2011). Aligned collagen is a prognostic signature for survival in human breast carcinoma. Am. J. Pathol. *178*, 1221–1232.

Cukierman, E., Pankov, R., Stevens, D.R., and Yamada, K.M. (2001). Taking cell-matrix adhesions to the third dimension. Science *294*, 1708–1712.

del Pozo, M.A., Balasubramanian, N., Alderson, N.B., Kiosses, W.B., Grande-Garcia, A., Anderson, R.G., and Schwartz, M.A. (2005). Phospho-caveolin-1 mediates integrin-regulated membrane domain internalization. Nat. Cell Biol. *7*, 901–908.

Doyle, A.D., Wang, F.W., Matsumoto, K., and Yamada, K.M. (2009). One-dimensional topography underlies three-dimensional fibrillar cell migration. J. Cell Biol. *184*, 481–490.

Drab, M. (2001). Loss of caveolae, vascular dysfunction, and pulmonary defects in Caveolin-1 gene-disrupted mice. Science *293*, 2449–2452.

Engler, A.J., Humbert, P.O., Wehrle-Haller, B., and Weaver, V.M. (2009). Multiscale modeling of form and function. Science *324*, 208–212.

Engler, A.J., Sen, S., Sweeney, H.L., and Discher, D.E. (2006). Matrix elasticity directs stem cell lineage specification. Cell *126*, 677–689.

Friedl, P., and Gilmour, D. (2009). Collective cell migration in morphogenesis, regeneration and cancer. Nat. Rev. Mol. Cell Biol. *10*, 445–457.

Gaggioli, C., Hooper, S., Hidalgo-Carcedo, C., Grosse, R., Marshall, J.F., Harrington, K., and Sahai, E. (2007). Fibroblast-led collective invasion of carcinoma cells with differing roles for RhoGTPases in leading and following cells. Nat. Cell Biol. *9*, 1392–1400.

Goetz, J.G., Joshi, B., Lajoie, P., Strugnell, S.S., Scudamore, T., Kojic, L.D., and Nabi, I.R. (2008a). Concerted regulation of focal adhesion dynamics by galectin-3 and tyrosine-phosphorylated caveolin-1. J. Cell Biol. *180*, 1261–1275.

Goetz, J.G., Lajoie, P., Wiseman, S.M., and Nabi, I.R. (2008b). Caveolin-1 in tumor progression: the good, the bad and the ugly. Cancer Metastasis Rev. *27*, 715–735.

Gonzalez-Munoz, E., Lopez-Iglesias, C., Calvo, M., Palacin, M., Zorzano, A., and Camps, M. (2009). Caveolin-1 loss of function accelerates glucose transporter 4 and insulin receptor degradation in 3T3-L1 adipocytes. Endocrinology *150*, 3493–3502.

Figure 7. Cav1-Dependent 3D Microenvironment Stimulates In Vivo Tumor Cell Invasion and Increases Metastatic Potency

(A) Orthotopic mammary gland allografts. (a) Experimental scheme. (b) Bioluminescence detection of TCs (representative images). Color scale depicts the photon flux (photons per second). (c) MPE-SHG of primary tumor explants. White and yellow arrows mark invading and encapsulated TCs. (d) Quantification of the angle of collagen fibers to the tumor boundary by SHG.

(B) Orthotopic mammary gland xenografts and tumor transplantation in nude mice. (a) Experimental scheme. (b) Representative extracted organs (left). Ex vivo quantification of the distribution of total and organ-specific metastatic foci (right). (c) Immunostaining of extracted tumors as indicated. (d) Quantification of intratumoral orientation of FN fibers plotted against the modal angle (set at 0°, left). Correlation analysis (right).

(C) Subcutaneous Matrigel injection of LM-4175 TCs plus the indicated pMEFs. (a) Experimental scheme. Immunoblot shows efficiency of p190 silencing and Cav1 expression. (b) Distribution of total and individual metastatic foci (ex vivo, day 70). (c) Representative images of primary tumors in vivo, extracted organs ex vivo, and immunostained tumors. (d) Correlation analysis.

Data are represented as mean ± standard error of the mean (SEM). See also Figure S7.

Grande-Garcia, A., Echarri, A., de Rooij, J., Alderson, N.B., Waterman-Storer, C.M., Valdivielso, J.M., and del Pozo, M.A. (2007). Caveolin-1 regulates cell polarization and directional migration through Src kinase and Rho GTPases. J. Cell Biol. *177*, 683–694.

Gratton, J.P., Lin, M.I., Yu, J., Weiss, E.D., Jiang, Z.L., Fairchild, T.A., Iwakiri, Y., Groszmann, R., Claffey, K.P., Cheng, Y.C., et al. (2003). Selective inhibition of tumor microvascular permeability by cavtratin blocks tumor progression in mice. Cancer Cell *4*, 31–39.

Hinz, B. (2010). The myofibroblast: paradigm for a mechanically active cell. J. Biomech. *43*, 146–155.

Karnoub, A.E., Dash, A.B., Vo, A.P., Sullivan, A., Brooks, M.W., Bell, G.W., Richardson, A.L., Polyak, K., Tubo, R., and Weinberg, R.A. (2007). Mesenchymal stem cells within tumour stroma promote breast cancer metastasis. Nature *449*, 557–563.

Krieg, M., Arboleda-Estudillo, Y., Puech, P.H., Kafer, J., Graner, F., Muller, D.J., and Heisenberg, C.P. (2008). Tensile forces govern germ-layer organization in zebrafish. Nat. Cell Biol. *10*, 429–436.

Levental, K.R., Yu, H., Kass, L., Lakins, J.N., Egeblad, M., Erler, J.T., Fong, S.F., Csiszar, K., Giaccia, A., Weninger, W., et al. (2009). Matrix crosslinking forces tumor progression by enhancing integrin signaling. Cell *139*, 891–906.

Mammoto, A., Huang, S., and Ingber, D.E. (2007a). Filamin links cell shape and cytoskeletal structure to Rho regulation by controlling accumulation of p190RhoGAP in lipid rafts. J. Cell Sci. *120*, 456–467.

Mammoto, T., Parikh, S.M., Mammoto, A., Gallagher, D., Chan, B., Mostoslavsky, G., Ingber, D.E., and Sukhatme, V.P. (2007b). Angiopoietin-1 requires p190 RhoGAP to protect against vascular leakage in vivo. J. Biol. Chem. *282*, 23910–23918.

Minn, A.J., Gupta, G.P., Siegel, P.M., Bos, P.D., Shu, W., Giri, D.D., Viale, A., Olshen, A.B., Gerald, W.L., and Massague, J. (2005). Genes that mediate breast cancer metastasis to lung. Nature *436*, 518–524.

Orimo, A., Gupta, P.B., Sgroi, D.C., Arenzana-Seisdedos, F., Delaunay, T., Naeem, R., Carey, V.J., Richardson, A.L., and Weinberg, R.A. (2005). Stromal fibroblasts present in invasive human breast carcinomas promote tumor growth and angiogenesis through elevated SDF-1/CXCL12 secretion. Cell *121*, 335–348.

Parton, R.G., and Simons, K. (2007). The multiple faces of caveolae. Nat. Rev. Mol. Cell Biol. *8*, 185–194.

Paszek, M.J., Zahir, N., Johnson, K.R., Lakins, J.N., Rozenberg, G.I., Gefen, A., Reinhart-King, C.A., Margulies, S.S., Dembo, M., Boettiger, D., et al. (2005). Tensional homeostasis and the malignant phenotype. Cancer Cell *8*, 241–254.

Provenzano, P.P., Eliceiri, K.W., Campbell, J.M., Inman, D.R., White, J.G., and Keely, P.J. (2006). Collagen reorganization at the tumor-stromal interface facilitates local invasion. BMC Med. *4*, 38.

Provenzano, P.P., Inman, D.R., Eliceiri, K.W., Trier, S.M., and Keely, P.J. (2008). Contact guidance mediated three-dimensional cell migration is regulated by Rho/ROCK-dependent matrix reorganization. Biophys. J. *95*, 5374–5384.

Razani, B., Engelman, J.A., Wang, X.B., Schubert, W., Zhang, X.L., Marks, C.B., Macaluso, F., Russell, R.G., Li, M., Pestell, R.G., et al. (2001). Caveolin-1 null mice are viable but show evidence of hyperproliferative and vascular abnormalities. J. Biol. Chem. *276*, 38121–38138.

Ronnov-Jessen, L., and Bissell, M.J. (2008). Breast cancer by proxy: can the microenvironment be both the cause and consequence? Trends Mol. Med. *15*, 5–13.

Sloan, E.K., Ciocca, D.R., Pouliot, N., Natoli, A., Restall, C., Henderson, M.A., Fanelli, M.A., Cuello-Carrion, F.D., Gago, F.E., and Anderson, R.L. (2009). Stromal cell expression of caveolin-1 predicts outcome in breast cancer. Am. J. Pathol. *174*, 2035–2043.

Sordella, R., Jiang, W., Chen, G.C., Curto, M., and Settleman, J. (2003). Modulation of Rho GTPase signaling regulates a switch between adipogenesis and myogenesis. Cell *113*, 147–158.

Williams, T.M., Sotgia, F., Lee, H., Hassan, G., Di Vizio, D., Bonuccelli, G., Capozza, F., Mercier, I., Rui, H., Pestell, R.G., et al. (2006). Stromal and epithelial caveolin-1 both confer a protective effect against mammary hyperplasia and tumorigenesis: Caveolin-1 antagonizes cyclin D1 function in mammary epithelial cells. Am. J. Pathol. *169*, 1784–1801.

Witkiewicz, A.K., Nguyen, K.H., Dasgupta, A., Kennedy, E.P., Yeo, C.J., Lisanti, M.P., and Brody, J.R. (2008). Co-expression of fatty acid synthase and caveolin-1 in pancreatic ductal adenocarcinoma: implications for tumor progression and clinical outcome. Cell Cycle *7*, 3021–3025.

Witkiewicz, A.K., Dasgupta, A., Sotgia, F., Mercier, I., Pestell, R.G., Sabel, M., Kleer, C.G., Brody, J.R., and Lisanti, M.P. (2009). An absence of stromal caveolin-1 expression predicts early tumor recurrence and poor clinical outcome in human breast cancers. Am. J. Pathol. *174*, 2023–2034.

Yamada, K.M., and Cukierman, E. (2007). Modeling tissue morphogenesis and cancer in 3D. Cell *130*, 601–610.

Yang, G., Timme, T.L., Naruishi, K., Fujita, T., Fattah el, M.A., Cao, G., Rajocopolan, K., Troung, L.D., and Thompson, T.C. (2008). Mice with cav-1 gene disruption have benign stromal lesions and compromised epithelial differentiation. Exp. Mol. Pathol. *84*, 131–140.

Zhao, X.H., Laschinger, C., Arora, P., Szaszi, K., Kapus, A., and McCulloch, C.A. (2007). Force activates smooth muscle alpha-actin promoter activity through the Rho signaling pathway. J. Cell Sci. *120*, 1801–1809.

Zhao, Y.Y., Liu, Y., Stan, R.V., Fan, L., Gu, Y., Dalton, N., Chu, P.H., Peterson, K., Ross, J., Jr., and Chien, K.R. (2002). Defects in caveolin-1 cause dilated cardiomyopathy and pulmonary hypertension in knockout mice. Proc. Natl. Acad. Sci. USA *99*, 11375–11380.

Zhong, C., Chrzanowska-Wodnicka, M., Brown, J., Shaub, A., Belkin, A.M., and Burridge, K. (1998). Rho-mediated contractility exposes a cryptic site in fibronectin and induces fibronectin matrix assembly. J. Cell Biol. *141*, 539–551.